Cross sections and reaction rates for $^{23}Na(p,n)^{23}Mg$, $^{27}Al(p,n)^{27}Si$, $^{27}Al(\alpha,n)^{30}P$, $^{29}Si(\alpha,n)^{32}S$, and $^{30}Si(\alpha,n)^{33}S$

D. S. Flynn, K. K. Sekharan, B. A. Hiller, H. Laumer, J. L. Weil, and F. Gabbard
University of Kentucky, Lexington, Kentucky 40506
(Received 15 March 1978)

The total neutron production cross sections for the $^{23}Na(p,n)^{23}Mg$, $^{27}Al(p,n)^{27}Si$, $^{27}Al(\alpha,n)^{30}P$, $^{29}Si(\alpha,n)^{32}S$, and $^{30}Si(\alpha,n)^{33}S$ reactions have been measured for bombarding energies from threshold to 6.3 MeV. The neutron detector was a 60-cm diameter sphere of polyethylene with eight $^{10}BF_3$ counters and was insensitive to the angle and energy of the emitted neutrons. Cross sections for inverse reactions have been obtained using the principle of detailed balance. The data have been used to determine parameters for statistical model calculations to facilitate extrapolation of cross sections to higher bombarding energies. These reactions are relevant to problems of nucleosynthesis and stellar evolution and to studies of radiation damage. Nucleosynthesis reaction rates, $N_A\langle\sigma v\rangle$, were determined for the reactions studied and are tabulated for temperatures ranging from 0.4×10^9 to 10.0×10^9 K.

[NUCLEAR REACTIONS ^{23}Na, $^{27}Al(p,n)$, $E_p=5.0-6.5$ MeV; ^{27}Al, ^{29}Si, $^{30}Si(\alpha,n)$, $E_\alpha=2.8-6.8$ MeV; measured $\sigma(E)$. $^{27}Si(n,p_0)$, $E_n=0-0.55$ MeV; $^{30}P(n,\alpha_0)$, $E_n=0.4-0.9$ MeV; ^{32}S, $^{33}S(n,\alpha)$, $E_n=0-2.3$ MeV; deduced $\sigma(E)$ from measured $\sigma(E)$ and detailed balance. $^{23}Mg(n,p)$, $E_n=0-3$ MeV; calculated $\sigma(E)$. Deduced nucleosynthesis reaction rates.]

I. INTRODUCTION

Synthesis of heavy nuclei from light ones (nucleosynthesis) in the interior of the stars is believed to be the origin of the heavier nuclei. Owing to the high temperatures (10^8 K for hydrostatic helium burning to 10^{10} K for explosive oxygen and silicon burning[1]) a series of nuclear reactions occurs, causing the formation of heavier nuclei from the lighter ones. In order to make quantitative predictions from a model of nucleosynthesis, many parameters such as temperature, elemental composition, and nuclear reaction cross sections must be determined. Since many of these cross sections can be measured directly with the facilities available at the University of Kentucky, we have begun a systematic study to measure total (p,n) and (α,n) cross sections and then determine the corresponding nucleosynthesis reaction rates. Woosley *et al.*[2] have calculated the reaction cross sections for neutrons, protons, and α particles incident on targets in the range of $A=20$ to $A=70$, using an optical model of the nucleus and statistical reaction theory. An objective of the present work is to compare experimental cross sections and their inverse cross sections with these calculated cross sections.

The cross sections for $^{23}Na(p,n)^{23}Mg$, $^{27}Al(\alpha,n)^{30}P$, $^{27}Al(p,n)^{27}Si$, $^{29}Si(\alpha,n)^{32}S$, and $^{30}Si(\alpha,n)^{33}S$ have been measured from threshold to about 6 MeV and will be presented and discussed in Sec. III. The experimental apparatus, target-thickness-measuring techniques, and measurement uncertainties are discussed in Sec. II. Inverse cross sections are presented and discussed in Sec. IV. The measured cross sections were fitted with statistical model calculations which are described in Sec. V. Finally, nucleosynthesis reaction rates are presented and compared to those of other authors in Sec. VI.

II. EXPERIMENTAL METHODS

The determination of a neutron production cross section requires a knowledge of the number of incident particles, the thickness of the target, and the number of outgoing neutrons. The targets were bombarded with a charged particle beam from a 6-MV Van de Graaff accelerator. The incident beam was stopped in a Faraday cup (with arrangements for electron suppression whenever necessary), and the number of charged particles was measured with a precision current integrator. The targets employed for the cross section measurements were evaporated onto high purity aluminum or carbon backings (500 or 10 $\mu g/cm^2$, respectively), and the target thicknesses were obtained by charged particle back scattering as described below. Neutron backgrounds were determined by bombarding blank aluminum and carbon backings. Other pertinent information about each target is given in the next section. The neutrons were detected with a sphere counter[3] consisting of eight $^{10}BF_3$ counters embedded radially in a polyethylene sphere of 60-cm diameter. The efficiency of this detector is constant within ±3%

for neutron energies ranging from 30 keV to 2 MeV and is equal to 0.55 ± (0.017)%.

The target thicknesses were measured by scattering α particles from the targets at low incident α-particle energies (1 to 3 MeV). A charged-particle scattering chamber[4] with accurate beam collimation and several silicon surface-barrier detectors was used to measure the yield of scattered α particles. Precision collimators mounted in front of each detector defined the solid angle subtended by each detector to an accuracy of 1%. Conventional electronics amplified, analyzed, and counted the detector pulses. The angle and energy dependence of the elastic scattering cross sections were observed to follow the Rutherford formula. It was assumed that, at these low energies, the yield was due entirely to Rutherford scattering; based on this assumption the target thicknesses were calculated from the scattered yields.

The precision in the target thickness measurements using the α-scattering technique was checked for several targets. Thicknesses were measured at several energies, positions, and angles. The standard error in the measurements of these targets was ≃6%. On the basis of these measurements, the standard error of all of the target thicknesses was estimated to be 6%.

The charge collection for both scattering and neutron measurements was done using a current integrator calibrated to an accuracy of < 1%. In the case of the neutron yield measurement with the sphere counter, the insulation for the Faraday cup was about 30 cm upstream with respect to the target position making the target chamber also part of the Faraday cup. The target thickness determination by α-particle scattering involved an experimental set up in which the Faraday cup was downstream with respect to the target position. In the latter case it was necessary to account for the stripping of the second electron from the helium ion when it passed through the target. For example, at 2.5 MeV the α-particle beam was estimated to consist of 96% He^{++} and 4% He^{+} after passing through the target.[5]

The error in the cross sections is thought to arise mainly from the uncertainty in the target thickness measurement. Other sources of errors come from uncertainties in the current integration, in the neutron yield due to counting statistics, in the efficiency of the neutron detector, and in the background neutron yield.

The error in the current integration is less than 1% and the statistical error in the neutron yield measurement was generally less than 2% (for cross sections less than a few millibarns the statistical uncertainties are larger). The efficiency of the neutron detector is known to 3%. The un-

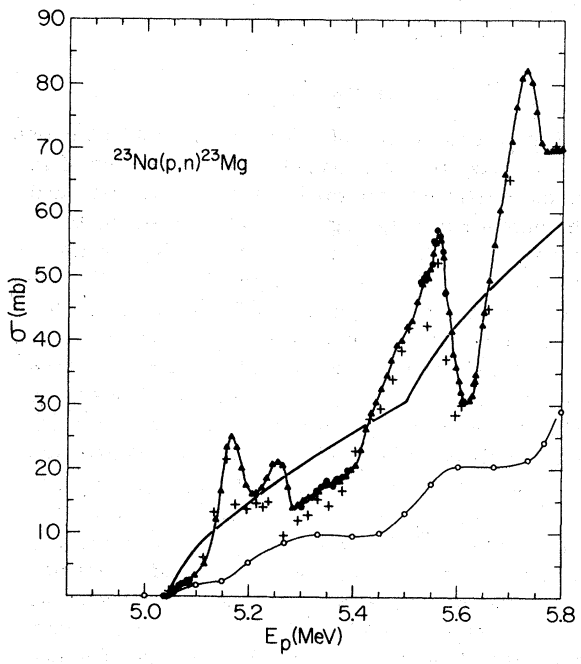

FIG. 1. ^{23}Na(p,n)^{23}Mg cross sections. ▲ and ●, results from NaOH-on-an-aluminum backing and NaOh-on-a-carbon backing, respectively. o and +, results of Ref. 6 and Ref. 7, respectively. The solid curve represents the results of our statistical model calculation [the calculated cross sections of Ref. 2 (not shown) are ~ 30% higher].

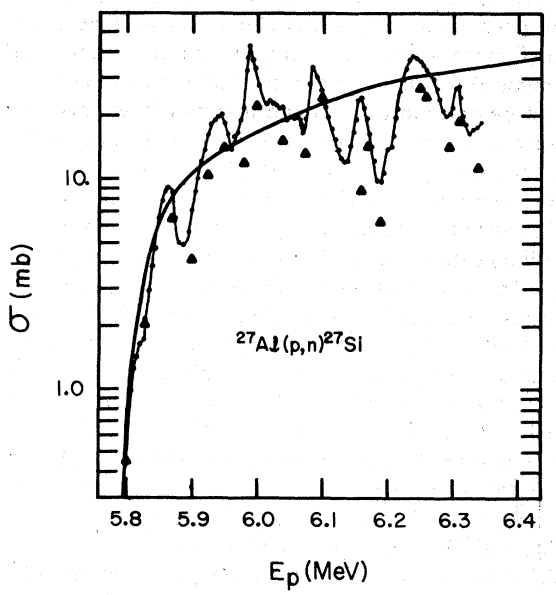

FIG. 2. ^{27}Al(p,n)^{27}Si cross sections. ▲, results of Ref. 8. The solid curve represents the results of our statistical model calculation (within the accuracy of this drawing, the calculated cross sections of Ref. 2 are identical to our calculated cross sections).

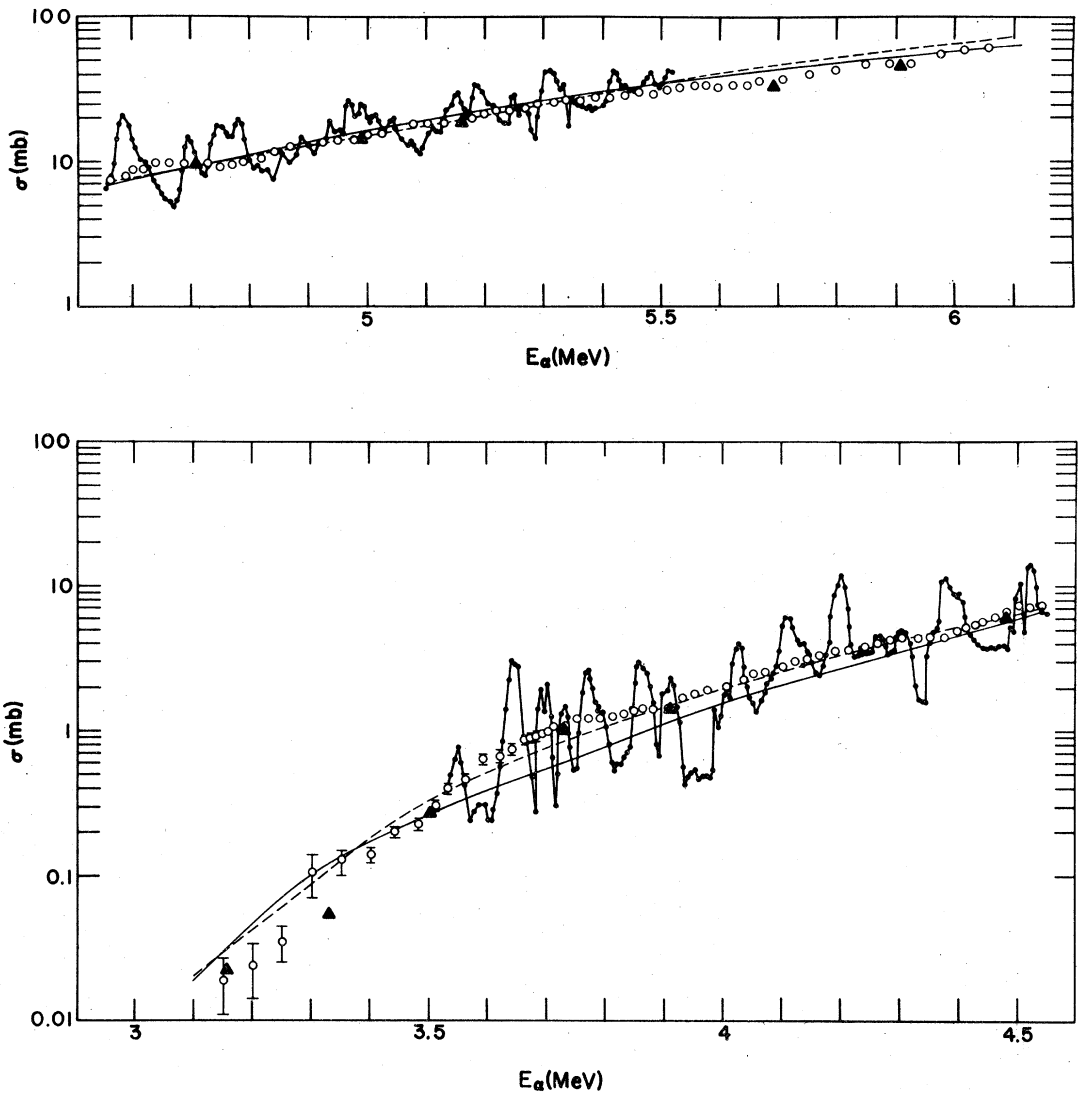

FIG. 3. $^{27}Sl(\alpha,n)^{30}P$ cross sections. o and ●, results from thick (442 $\mu g/cm^2$) and thin (27 $\mu g/cm^2$) targets, respectively. ▲, results of Ref. 10. The solid curve represents the results of our statistical model calculation, and the dashed curve represents the calculated cross sections of Ref. 2.

certainty in the determination of the background neutrons is normally 3 to 4% or less; when the cross sections being measured become small or when the reaction producing the background neutrons resonates [especially $^{13}C(\alpha,n)^{16}O$)] then this uncertainty becomes larger. The standard error in the cross section for each reaction was taken to be the square root of the sum of the squares of the errors mentioned above and is generally about 8%.

III. EXPERIMENTAL RESULTS

A. $^{23}Na(p,n)^{23}Mg$

The neutron yield from a NaOH target evaporated onto an aluminum backing was measured from the $^{23}Na(p,n)$ threshold to 5.8 MeV in steps of 10 keV. It was not possible to determine the thickness of this target by elastic scattering since α particles scattered from the aluminum backing

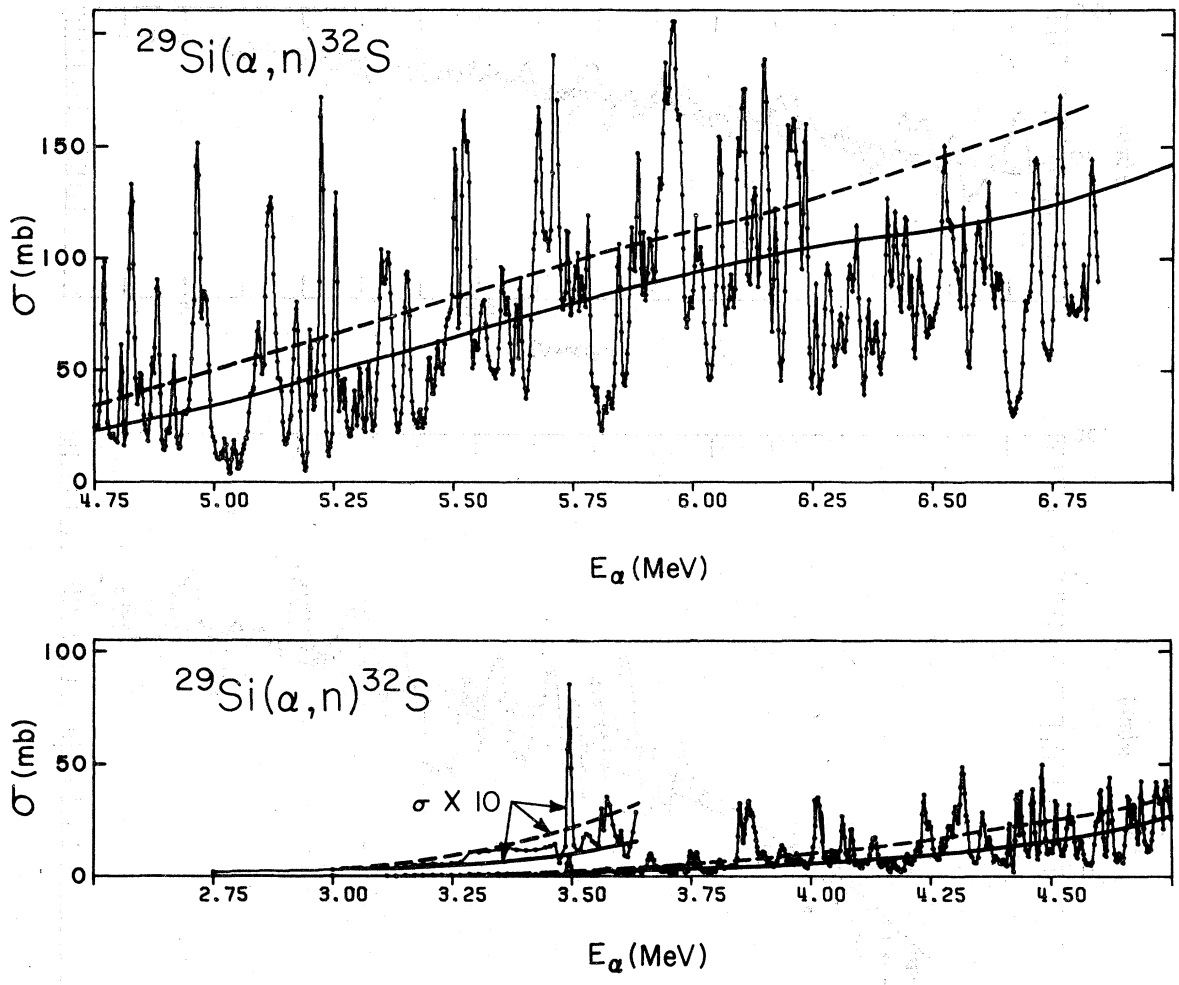

FIG. 4. $^{29}Si(\alpha,n)^{32}S$ cross sections. The solid curve represents the results of our statistical model calculation, and the dashed curve represents the calculated cross sections of Ref. 2.

could not be distinguished from those scattered from the sodium. Therefore the $^{23}Na(p,n)$ cross section was normalized with a NaOH target on a carbon backing whose sodium thickness was measured by α scattering. The sodium thicknesses were approximately 20 $\mu g/cm^2$ in both targets.

Figure 1 shows the cross sections obtained with the NaOH-on-carbon target and with the NaOH-on-aluminum target. This excitation function has been measured before by other methods.[6,7] For comparison, the results of Refs. 6 and 7 are also shown in Fig. 1. Our cross sections are in agreement with those of Ref. 7. Resonance structure in the $^{23}Na(p,n)$ reaction ($\gtrsim$50 keV wide) was not significantly distorted by our experimental resolution of ~5 keV.

B. $^{27}Al(p,n)^{27}Si$ and $^{27}Al(\alpha,n)^{30}P$

Three targets of thickness 27, 30, and 442 $\mu g/cm^2$ were used in these measurements. The thin targets were made by evaporating 99.9% pure ^{27}Al powder onto carbon backings, and the thick target was a self-supporting foil which was 99.7% pure ^{27}Al. The thickness of the 442-$\mu g/cm^2$ target was obtained by weighing the foil and measuring its area. One of the thinner targets was used in the $^{27}Al(p,n)$ experiment, but the $^{27}Al(\alpha,n)$ yields were measured with both thick and thin targets. Using the thick target enabled a more accurate measurement of the small cross sections near the $^{27}Al(\alpha,n)$ threshold.

Results of the $^{27}Al(p,n)$ measurements are shown

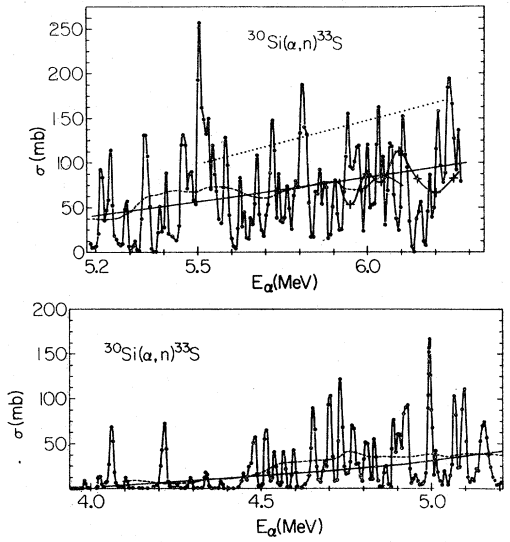

FIG. 5. ^{30}Si$(\alpha,n)^{33}$S cross sections. +, results of Ref. 15. The solid curve represents the results of our statistical model calculation. The dashed curve represents the cross sections obtained by averaging the measured cross section over a 250 keV interval. The dotted line represents the cross sections calculated by Ref. 2.

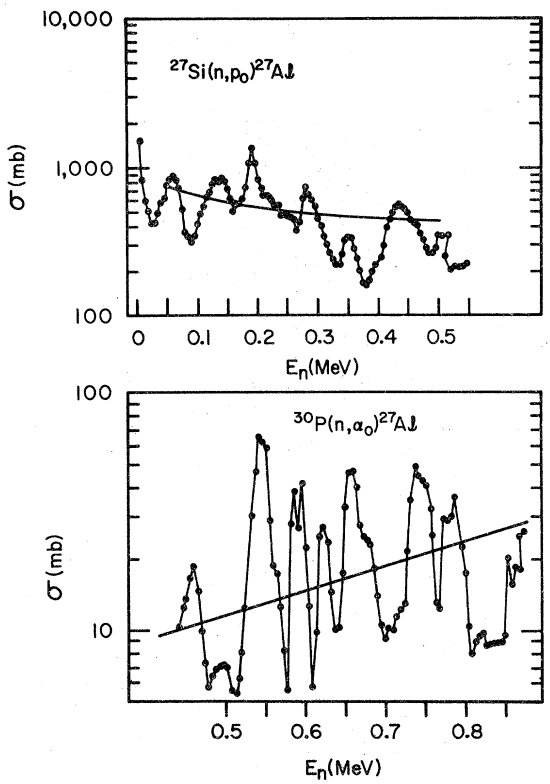

FIG. 6. ^{27}Si $(n,p_0)^{27}$Al and ^{30}P$(n,\alpha_0)^{27}$Al cross sections obtained from the measured ^{27}Al$(p,n)^{27}$Si and ^{27}Al$(\alpha,n)^{30}$P cross sections by detailed balance. The smooth curve represents the results of our statistical model calculation.

in Fig. 2. The ^{27}Al(p,n) excitation function has previously been measured by an activation technique.[8] For comparison, these results are also shown in Fig. 2. This reaction was measured[3] in our laboratory for the purpose of testing the spherical neutron detector. When these data were reported,[3] it was pointed out that the ^{27}Al(p,n) cross sections measured with the spherical detector were 7 to 25% higher than those of Ref. 8 and further measurements were planned to check this discrepancy. One reason that we remeasured this reaction was to further investigate this discrepancy in hopes of gaining more confidence in the accuracy of the spherical detector. The present results are in agreement with our previous results, even though the experiments were different in several respects. Target thicknesses were determined by weighing in the original work and by elastic scattering in the latter, and the target fabrication and data analysis were done independently in the two experiments. The efficiency of the spherical detector has recently been rechecked by counting photoneutrons from the radium-beryllium source NBS-II.[9]

Results of the ^{27}Al(α,n) measurements are shown in Fig. 3. Values of the cross sections obtained with the thick target agree well with those obtained with the thin target. An excitation function for this reaction has also been obtained by Howard *et al.*[10] using a thick target. For comparison to the present work, the results of Ref. 10 are also shown in Fig. 3.

C. ^{29}Si$(\alpha, n)^{32}$S and ^{30}Si$(\alpha, n)^{33}$S

Neutron yields from enriched ^{29}Si and ^{30}Si targets were measured for the incident α-particle-energy range from near threshold to 6.8 MeV for ^{29}Si and 6.25 MeV for ^{30}Si, and the resulting cross sections are shown in Figs. 4 and 5, respectively. The targets were enriched to 95.28 and 95.55%, respectively. The abundance of ^{28}Si in the target materials was about 4%. Other contaminants were less than 0.4% of the samples. The presence of ^{28}Si did not interfere with the neutron yield measurement as the Q value for ^{28}Si$(\alpha,n)^{31}$S is -8.144 MeV. The targets were prepared by heating a mixture of SiO_2 and tantulum powder by electron bombardment and evaporating the Si onto a carbon backing.

Targets of about 9 μg/cm^2 of silicon on 10-μg/cm^2 carbon backings were used with one ex-

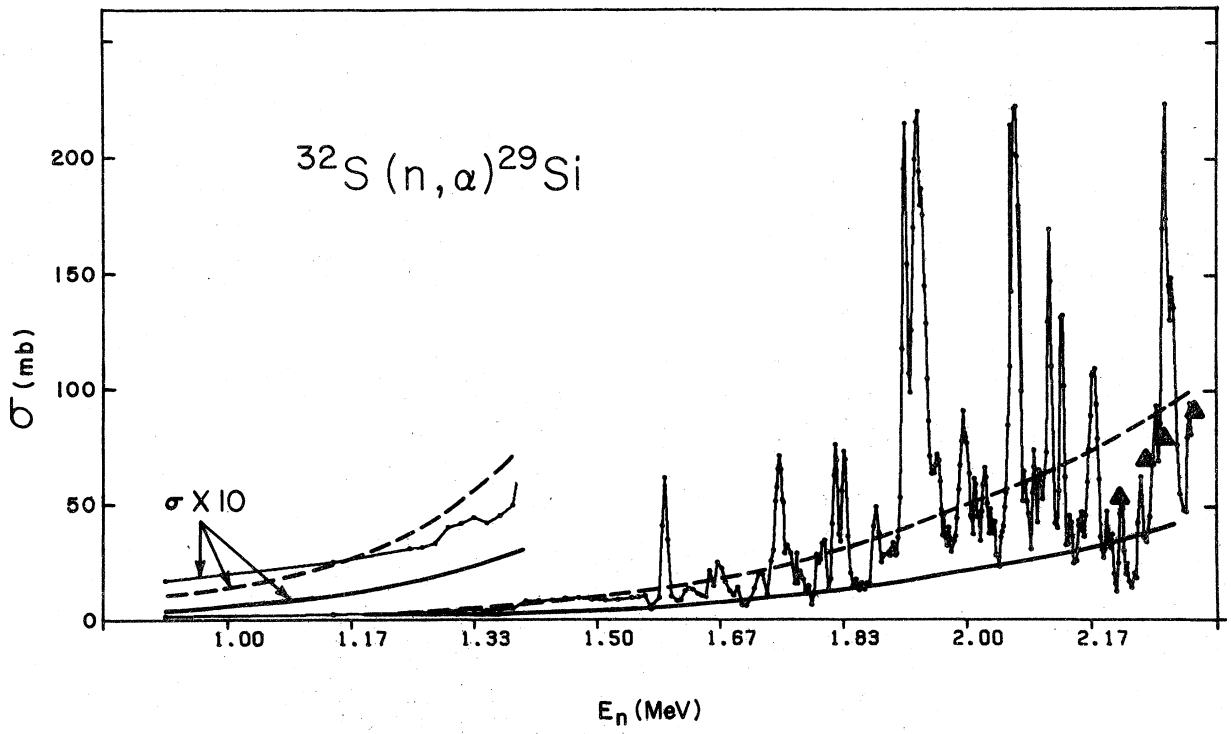

FIG. 7. $^{32}S(n,\alpha)^{29}Si$ cross sections obtained from the measured $^{29}Si(\alpha,n)^{32}S$ cross sections by detailed balance. ▲, results of Ref. 18. The solid curve represents the results of our statistical model calculation. The dashed curve represents the calculated cross sections of Ref.2.

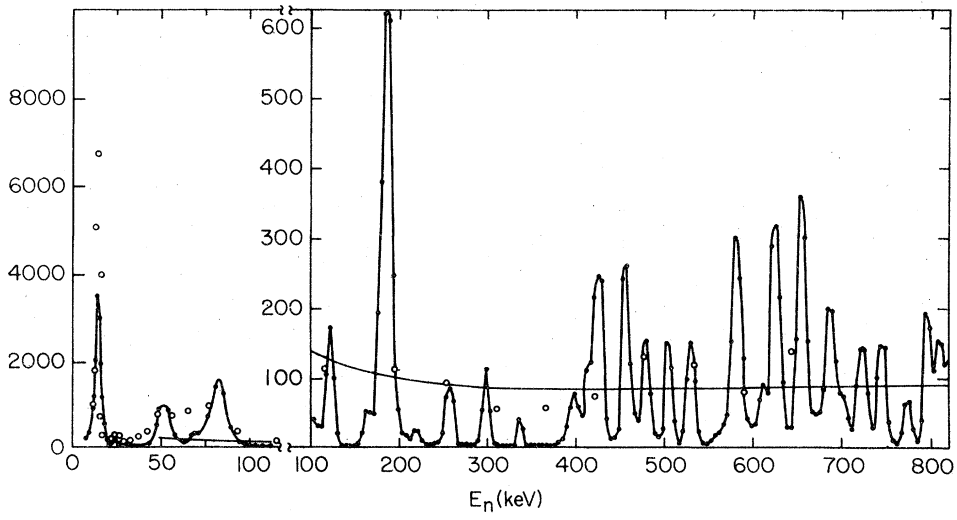

FIG. 8. $^{33}S(n,\alpha)^{30}Si$ cross sections obtained from the measured $^{30}Si(\alpha,n)^{33}S$ cross sections by detailed balance. o, results of Ref. 19. The smooth curve represents the results of our statistical model calculation.

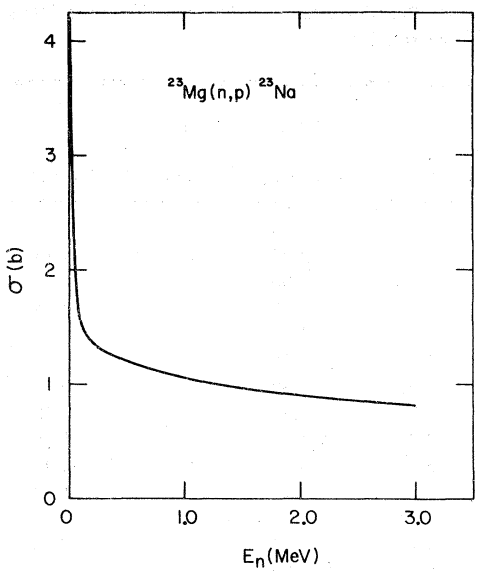

FIG. 9. ^{23}Mg$(n,p)^{23}$Na cross sections calculated with optical model parameters which were obtained by fitting the measured ^{23}Na$(p,n)^{23}$Mg cross sections.

ception. Since the ^{29}Si(α,n) threshold is relatively low in energy, there is a wide range of energies in which the cross section is very small. In order to more accurately measure this part of the excitation function, a thick (113 μg/cm^2) target was fabricated by depositing ^{29}Si onto a ^{58}Ni disk. The ^{29}Si(α,n) excitation function was measured with this thick target from 2.75 to 3.46 MeV and with a thin target above 3.46 MeV. The ^{30}Si(α,n) cross section was obtained entirely with a thin target.

Background neutrons from the carbon foils were a problem in these two experiments. The ^{13}C$(\alpha,n)^{16}$O excitation function was measured with blank carbon foils. The raw Si(α,n) data were then corrected by subtracting a background which varied as the measured ^{13}C(α,n) excitation function. At the lower energies, peaks in the raw Si(α,n) data could easily be identified as the large ^{13}C(α,n) resonances[11,12]; the amount of the ^{13}C(α,n) background subtracted from the Si(α,n) data was adjusted to remove these large peaks.

Gibbons and Macklin[13] and Balakrishnan *et al*[14] have measured parts of the ^{29}Si(α,n) excitation function. The ^{29}Si(α,n) cross sections obtained in the present experiment are about twice as large as those obtained by Gibbons and Macklin. The cross sections published by Balakrishnan *et al.* appear to be contaminated by a ^{13}C$(\alpha,n)^{16}$O background [the wide structure they observe below 3.5 MeV can be identified as resonances in ^{13}C$(\alpha,n)^{16}$O]. The results of the present experiment agree with those of Balakrishnan *et al.* at 3.85 MeV where the ^{13}C(α,n) cross section is very small. McCamis *et al.*[15] have measured angular distributions for ^{30}Si$(\alpha,n)^{33}$S with time of flight techniques. They then integrated the differential cross section to determine the total ^{30}Si(α,n) cross section. A portion of their results is also shown for comparison in Fig. 5.

IV. INVERSE CROSS SECTIONS

The principle of detailed balance[16] was used to compute the cross sections for the (n,p) and (n,α) reactions which are inverse to the measured (p,n) and (α,n) cross sections. It is always possible to calculate the inverse partial cross section, (n,p_0) or (n,α_0), on the energy interval below the threshold for the first excited state of the residual (target for the inverse reaction) nucleus. The first excited states of the residual nuclei for the reactions reported here are at 0.45, 0.78, 0.68, 2.23, and 0.84 for ^{23}Mg, ^{27}Si, ^{30}P, ^{32}S, and ^{33}S, respectively.[17] Since there is considerable structure in all but the ^{23}Na$(p,n)^{23}$Mg reaction, the (n,p_0) and (n,α_0) cross sections have been determined using detailed balance for the other four reactions in the interest of providing good resolution cross sections for these reactions. The results of these computations are shown in Figs. 6–8.

TABLE I. Optical model parameters.

	Real potential				Imaginary potential				Spin orbit[a]
Projectile	V_0 (MeV)	$\Delta V/E^{c.m.}$	R (fm)	a (fm)	W_0 (MeV)	$\Delta W/E^{c.m.}$	R_D (fm)	a_D (fm)	V_{so} (Mev)
Neutron	42.4	−0.267	1.25	0.65	9.52	−0.053	1.25	0.66	6.0
Proton	50.0[b]	−0.330	1.25	0.65	7.5	0.000	1.25	0.7	5.5
α particle	80.4	−0.267	1.48	0.59	10.0	−0.053	1.48	0.3	0.0

[a] R_{so} and a_{so} were equal to R and a, respectively.

[b] Except for ^{23}Na, where V_0 = 53.8 MeV.

It is generally not possible to compute the inverse total cross section from the measured forward total cross section using detailed balance. In cases where the forward reaction is not too endothermic and excited states play a very minor role in either direction, the computed inverse *partial* cross section connecting ground states is a reasonably accurate estimate of the inverse *total* cross section. For example, the $^{32}S(n,\alpha)^{29}Si$ and $^{33}S(n,\alpha)^{30}Si$ total cross sections can be obtained quite accurately up to neutron energies of 2.23 and 0.84 MeV, respectively, because the partial (n,α) cross sections to excited states of ^{29}Si and ^{30}Si are negligible compared to the (n,α_0) cross section. Part of the $^{32}S(n,\alpha)^{29}Si$ excitation function has been measured directly by Hürliman *et al.*[18] and is shown in Fig. 7 along with the present results. The $^{33}S(n,\alpha)^{30}Si$ excitation function has been measured directly by Auchampaugh *et al.*[19] and is shown in Fig. 8 for comparison with present results.

In cases where the reaction is highly endothermic such as $^{23}Na(p,n)^{23}Mg$, many excited states are populated by the inverse reaction, and detailed balance is of little help in determining the inverse total cross section. One way to obtain the total (n,p) cross section in such a case is through a calculation using the statistical model with the optical model parameters derived by fitting the forward cross section. One must be wary of using this method because the forward cross section does not measure the transmission coefficients for the excited states of the target. However, lacking a better alternative, this method was used to obtain the cross section shown in Fig. 9 for $^{23}Mg(n,p)^{23}Na$.

V. CROSS SECTION CALCULATIONS

Cross sections have been calculated for each reaction studied using the statistical model.[20] The results of these calculations are represented by the smooth solid curves shown in Figs. 1–9. Some details of the calculation are given in the next paragraph. Starting values of optical model parameters (Table I) were taken from Ref. 21, and then adjusted to fit the average of the measured cross sections. Once determined, the parameters were fixed for all of the computations (with the one exception footnoted in Table I). The fact that one set of "reasonable" parameters gave fits to all of the measured cross sections is interesting in its own right. However, the primary reason for our calculations was to enable us to more accurately extrapolate the cross sections to higher energies and, in the cases of $^{29}Si(\alpha,n)$ and

TABLE II. Reaction rates for $^{23}Na\ (p,n)\ ^{23}Mg$ and ^{23}Mg-$(n,p)\ ^{23}Na$ (Ref. 26).

	$^{23}Na\ (p,n)\ ^{23}Mg$				
Temp. (10^9 K)	Exp.[a]	Exp. + Calc.[b]	Ref. 24	Ref. 2	n[c]
0.4	1.14	1.14		2.76	-53
0.5	2.06	2.06	1.38	4.14	-41
0.6	3.06	3.06			-33
0.7	2.10	2.10		3.44	-27
0.8	4.99	4.99			-23
0.9	1.26	1.26			-19
1.0	6.68	6.69		9.55	-17
1.5	9.96	9.98		13.00	-09
2.0	1.22	1.31		1.56	-04
2.5	3.38	3.92		4.47	-02
3.0	1.41	1.78		1.97	00
3.5	1.98	2.75			01
4.0	1.41	2.14		2.26	02
4.5	0.634	1.06			03
5.0	2.11	3.82	3.23	3.93	03
6.0	1.23	2.59		2.62	04
7.0	0.419	1.01		1.01	05
8.0	1.02	2.76		2.75	05
9.0	2.01	6.02			05
10.0	0.340	1.11		1.09	06

	$^{23}Mg\ (n,p)\ ^{23}Na$				
Temp. (10^9 K)	Calc.[d]	Ref. 7	Ref. 25	Ref. 2[e]	n[c]
0.4	3.93				
0.5	4.07	3.46	1.06	5.17	08
0.6	4.20				08
0.7	4.32				08
0.8	4.44	4.24	1.45	5.30	08
0.9	4.55				08
1.0	4.67	4.71	1.78	5.40	08
1.5	5.17	5.74	2.66	5.65	08
2.0	5.61	6.56	3.50	5.89	08
2.5	5.99	7.22	4.27	6.11	08
3.0	6.33	7.74	4.96	6.32	08
3.5	6.64				08
4.0	6.91	8.49	6.11	6.68	08
4.5	7.16				08
5.0	7.40	8.97	7.01	6.96	08
6.0	7.81				08
7.0	8.19				08
8.0	8.52				08
9.0	8.83				08
10.0	9.11				08

[a] Reaction rates obtained from experimental cross sections.
[b] Reaction rates obtained from experimental plus calculated cross sections.
[c] Obtain reaction rates in $(cm^3/mole)/sec$ by multiplying by 10^n.
[d] Reaction rates obtained from calculated cross sections.
[e] These rates are not actually listed in Ref. 2 but were calculated for us by S. E. Woosley.

TABLE III. Reaction rates for $^{27}Al(p, n)^{27}Si$, $^{27}Al(\alpha,n)^{30}P$, $^{29}Si(\alpha,n)^{32}S$, $^{32}S(n, \alpha)^{29}Si$, $^{30}Si(\alpha, n)^{33}S$, and $^{33}S(n,\alpha)^{30}Si$ (Ref. 26).

Temp. (10^9 K)	Exp.[a]	Exp. + Calc.[b]	Ref. 2	n[c]
		$^{27}Al\ (p, n)\ ^{27}Si$		
0.4	3.33	3.33	14.2	-63
0.5	4.75	4.75	15.5	-49
0.6	1.31	1.31	3.52	-39
0.7	7.32	7.32	17.0	-33
0.8	8.41	8.43	17.5	-28
0.9	7.24	7.27	13.9	-24
1.0	1.02	1.03	1.84	-20
1.5	2.68	2.83	4.28	-11
2.0	1.29	1.48	2.09	-06
2.5	0.794	1.01	1.37	-03
3.0	5.51	7.90	10.3	-02
3.5	1.11	1.79	2.29	00
4.0	1.02	1.86	2.34	01
4.5	0.568	1.16	1.43	02
5.0	2.20	4.99	6.06	02
6.0	1.62	4.51	5.31	03
7.0	0.652	2.17	2.49	04
8.0	1.80	7.07	7.88	04
9.0	0.390	1.77	1.92	05
10.0	0.711	3.66	3.87	05
		$^{27}Al\ (\alpha, n)\ ^{30}P$		
0.4	3.05	3.05	7.69	-29
0.5	1.54	1.54	3.66	-22
0.6	4.82	4.82	10.7	-18
0.7	8.29	8.29	17.2	-15
0.8	2.34	2.34	4.49	-12
0.9	1.98	1.98	3.47	-10
1.0	7.16	7.16	11.5	-09
1.5	4.60	4.60	5.08	-04
2.0	1.46	1.46	1.35	-01
2.5	5.15	5.20	4.60	00
3.0	5.93	6.12	5.46	01
3.5	3.52	3.80	3.49	02
4.0	1.37	1.58	1.49	03
4.5	3.95	4.96	4.82	03
5.0	0.926	1.28	1.27	04
6.5	3.30	5.71	5.81	04
7.0	0.807	1.76	1.81	05
8.0	1.55	4.26	4.38	05
9.0	2.55	8.66	8.90	05
10.0	0.374	1.55	1.59	06
		$^{29}Si\ (\alpha, n)\ ^{32}S$		
0.8		3.05	10.2	-08
0.9		4.96	14.8	-07
1.0	0.607	5.02	13.4	-06
1.5	0.760	1.26	1.87	-02
2.0	1.06	1.25	1.36	00
2.5	2.46	2.64	2.55	01
3.0	2.25	2.32	2.20	02
3.5	1.18	1.20	1.15	03
4.0	4.26	4.33	4.29	03
4.5	1.20	1.22	1.25	04
5.0	2.79	2.89	3.04	04
6.0	1.02	1.12	1.22	05
7.0	2.64	3.06	3.44	05
8.0	5.39	6.75	7.71	05
9.0	0.936	1.28	1.47	06
10.0	1.45	2.15	2.48	06
		$^{32}S\ (n, \alpha)\ ^{29}Si$		
0.5		3.83	16.3	2
0.6		4.15	18.8	2
0.7	0.027	6.86	22.5	2
0.8	0.163	9.18	27.5	2
0.9	0.067	1.25	3.43	3
1.0	0.208	3.71	4.37	3
1.5	0.702	1.16	1.70	4
2.0	4.98	5.95	6.41	4
2.5	1.83	2.06	1.99	5
3.0	4.59	5.28	5.00	5
3.5	0.90	1.10	1.05	6
4.0	1.48	1.96	1.93	6
4.5	2.16	3.17	3.19	6
5.0	2.91	4.72	4.88	6
6.0	4.43	8.84	9.59	6
7.0	0.58	1.41	1.61	7
8.0	0.70	2.04	2.41	7
9.0	0.79	2.71	3.34	7
10.0	0.85	3.40	4.37	7
		$^{30}Si\ (\alpha, n)\ ^{33}S$		
0.4	8.83	8.83	4.65	-37
0.7	5.49	5.49	2.89	-18
1.0	1.64	1.64	0.974	-10
1.5	1.04	1.04	0.733	-04
2.0	8.63	8.63	6.77	-02
2.5	5.07	5.07	4.29	00
3.0	7.90	7.94	7.15	01
4.0	2.56	2.64	2.63	03
5.0	2.10	2.28	2.47	04
6.0	8.47	9.79	11.6	04
8.0	4.70	6.87	8.68	05
10.0	1.26	2.32	3.07	06
		$^{33}S\ (n, \alpha)\ ^{30}Si$		
0.4	6.90	6.90	3.18	07
0.5	6.90	6.90	3.13	07
0.6	6.76	6.76	3.10	07
0.7	6.55	6.55	3.09	07
0.8	6.32	6.32	3.09	07
0.9	6.08	6.08	3.09	07
1.0	5.87	5.87	3.11	07
1.5	5.15	5.18	3.27	07

TABLE III. (*Continued*)

Temp. (10^9 K)	Exp.[a]	Exp. + Calc.[b]	Ref. 2	n[c]	Temp. (10^9 K)	Exp.[a]	Exp. + Calc.[b]	Ref. 2	n[c]
	^{33}S (n, α) ^{30}Si					^{33}S (n, α) ^{30}Si			
2.0	4.80	4.95	3.55	07	5.0	3.66	6.34	6.23	07
2.5	4.60	5.00	3.90	07	6.0	3.30	7.04	7.26	07
3.0	4.42	5.16	4.30	07	7.0	2.97	7.75	8.29	07
3.5	4.23	5.40	4.74	07	8.0	2.69	8.47	9.29	07
4.0	4.05	5.70	5.22	07	9.0	2.43	9.15	10.2	07
4.5	3.86	6.02	5.72	07	10.0	2.21	9.81	11.1	07

[a] Reaction rates obtained from experimental cross sections.

[b] Reaction rates obtained from experimental plus calculated cross sections.

[c] Obtain reaction rates in (cm^3/mole)/sec by multiplying by 10^n.

^{32}S(n, α), to lower energies. As will be discussed in the next section, at some temperatures the measured cross sections do not extend far enough to yield accurate reaction rates.

The cross sections were calculated in a conventional manner with the statistical-model code ALTE.[22] Cross sections for photon decay of the compound nucleus were assumed to be negligible compared to cross sections for particle decay. Transmission functions in the particle (neutron, proton, and α) channels were evaluated with the optical-model potential defined in Ref. 21. A derivative Woods-Saxon form was adopted for the imaginary part of the potential. Values of the parameters used in the present calculations are listed in Table I (see Ref. 21 for definitions of the parameters). Bound state properties used in the statistical-model calculations are from Endt and van der Leun.[17]

VI. REACTION RATES

Reaction rates were determined by numerically integrating the expression[23]

$$\langle \sigma v \rangle = [(\tfrac{1}{8})\pi M(kT)^3]^{-1/2} \int_0^\infty E\sigma(E) \exp(-E/kT) dE ,$$

where $\sigma(E)$ is the total cross section for the reaction whose rate is being calculated, E is the center-of-mass kinetic energy, T is the temperature, M is the reduced mass, and k is Boltzmann's constant. Tables II and III list the reaction rates for all of the measured reactions and their inverses [except for ^{27}Si$(n, p_0)^{27}$Al and ^{30}P$(n, \alpha_0)^{27}$Al where not enough of the excitation functions were obtained]. The columns labeled "Exp." are reaction rates obtained from the experimental cross sections only, i.e., $\sigma(E)$ is assumed zero at energies where the cross sections were not determined experimentally. The columns labeled "Exp. and Calc." are reaction rates obtained from the experimental cross sections extended with calculated cross sections. Also listed in Tables II and III are reaction rates published by other authors.[2,7,24,25] The reaction rates listed in Table II for Ref. 24 were computed from the formula presented in Ref. 24. Since the formula in Ref. 24 enabled us to calculate only the stellar reaction rate, we converted to a laboratory reaction rate by multiplying by the ratio of the laboratory to stellar reaction rate obtained from the calculated reaction rates of Ref. 2.

VII. CONCLUSION

The results are in reasonably good agreement with the calculated reaction rates of Woosley *et al.*[2] Woosley's low-temperature reaction rates are systematically high by a factor of 2 or more; however, agreement at higher temperatures ($>10^9$ *K*) is better, and the largest difference is about 30%. An exception is the reaction rate for ^{30}Si$(\alpha, n)^{33}$S for which the rate obtained from our measurements is higher than Woosley's calculated value by a factor of about 2 at low temperature. The ^{30}Si$(\alpha, n)^{33}$S cross section below 4.4 MeV is small and subject to background subtraction errors. Further investigations at bombarding energies near threshold is suggested with special attention to assure that carbon deposit on target materials is kept at a minimum. The ^{13}C buildup is a

particularly severe problem for α induced reactions.

ACKNOWLEDGMENTS

The authors wish to thank Dr. W. A. Fowler and Dr. S. E. Woosley for helpful discussions and correspondence. Mr. Andrew Hurt and Dr. Robert Hershberger helped with the data collection and reduction. We also want to thank Professor Bernard Kern for help with the calibration and source preparation. This work was supported in part by a grant from the National Science Foundation.

[1]S. Chandrasekhar, *An Introduction to the Study of Stellar Structure* (Dover, New York, 1939), p. 469.

[2]S. E. Woosley, W. A. Fowler, J. A. Holmes, and B. A. Zimmerman, California Institute of Technology, Report No. OAP-422 (unpublished).

[3]K. K. Sekharan, H. Laumer, B. D. Kern, and F. Gabbard, Nucl. Instrum. Methods 133, 253 (1976).

[4]R. L. Schulte, Ph.D. thesis, University of Kentucky, 1970 (unpublished).

[5]J. B. Marion and F. C. Young, *Nuclear Reaction Analysis* (North Holland, Amsterdam, 1968).

[6]J. P. Blaser, F. Boehm, P. Marmier, and P. Scherrer, Helv. Phys. Acta. 24, 465 (1951).

[7]F. M. Mann, D. W. Kneff, Z. E. Switkowski, and S. E. Woosley, Nucl. Phys. A256, 163 (1976).

[8]I. F. Bubb, J. M. Poate, and R.H. Spear, Nucl. Phys. 65, 655 (1965).

[9]L. F. Curtiss and A. Carson, Phys. Rev. 76, 1412 (1949).

[10]A. J. Howard, H. B. Jesen, M. Rios, W. A. Fowler, and B. A. Zimmerman, Ap. J. 188, 131 (1974).

[11]K. K. Sekharan, A. S. Divatia, M. K. Mehta, S. S. Kerekatte, and K. M. Namiar, Phys. Rev. 156, 1187 (1967).

[12]J. K. Bair and F. X. Haas, Phys. Rev. C 7, 1356 (1973).

[13]J. H. Gibbons and R. L. Macklin, Phys. Rev. 114, 571 (1959).

[14]M. Balakrishnan, M. K. Mehta, A. S. Divatia, and S. Kailas, Phys. Rev. C 11, 54 (1975).

[15]R. H. McCamis, G. A. Moss, T. H. Hall, and J. M. Cameron, University of Alberta, Edmonton, Alberta, Canada, private communication.

[16]E. Segre, *Nuclei and Particles* (Benjamin, New York, 1964), p. 435.

[17]P. M. Endt and C. van der Leun, Nucl. Phys. A214, 1 (1973).

[18]T. Hürlimann, and P. Huber, Helv. Phys. Acta 28, 33 (1959).

[19]G. F. Auchampaugh, J. Halperin, R. L. Macklin, and W. M. Howard, Phys. Rev. C 12, 1126 (1975).

[20]L. Wolfenstein, Phys. Rev. 82, 690 (1951); W. Hauser and H. Feshbach, *ibid.* 87, 366 (1952); P. A. Moldauer, Rev. Mod. Phys. 36, 1079 (1964).

[21]C. M. Perey and F. G. Perey, At. Data Nucl. Data Tables 17, 1 (1976).

[22]W. R. Smith, Comp. Phys. Commun. 1, 106, 181 (1969).

[23]W. A. Fowler, Q. J. R. Astron. Soc. 15, 82 (1974).

[24]W. A. Fowler, G. R. Caughlan, and B. A. Zimmerman, Ann. Phys. Astro. Astrophys. 13, 69 (1975).

[25]J. W. Truran, Astrophys. Space Sci. 18, 306 (1972); S. E. Woosley, J. A. Holmes, W. A. Fowler, and B. A. Zimmerman (unpublished).

[26]See AIP document No. PAPS18-1566-21 for 21 pages of measured cross section values. Order by PAPS number and journal reference from American Institute of Physics. Physics Auxiliary Publication Service, 335 East 45th Street, New York, N.Y. 10017. The price is $1.50 for microfiche, or $5 for photocopies. Airmail additional. Make checks payable to the American Institute of Physics, This material also appears in *Current Physics Microfilm*, the monthly microfilm edition of the complete set of journals published by AIP, on the frames immediately following this journal article.